LAWRENCE
LIVERMORE
NATIONAL
LABORATORY

LLNL-CONF-817968

Comparing Plasma Conditions in Short-Pulse-Heated Foils via Fine-Structure X-ray Emission (paper)

B. F. Kraus, A. Chien, L. Gao, K. W. Hill, M. Bitter, P. C. Efthimion, H. Chen, M. B. Schneider, A. Moreau, R. Hollinger, S. Wang, H. Song, J. Rocca

December 29, 2020

Virtual 23rd Topical Conference on High-Temperature Plasma Di- agnostics
Virtual , United States
December 14, 2020 through December 17, 2020

Disclaimer

This document was prepared as an account of work sponsored by an agency of the United States government. Neither the United States government nor Lawrence Livermore National Security, LLC, nor any of their employees makes any warranty, expressed or implied, or assumes any legal liability or responsibility for the accuracy, completeness, or usefulness of any information, apparatus, product, or process disclosed, or represents that its use would not infringe privately owned rights. Reference herein to any specific commercial product, process, or service by trade name, trademark, manufacturer, or otherwise does not necessarily constitute or imply its endorsement, recommendation, or favoring by the United States government or Lawrence Livermore National Security, LLC. The views and opinions of authors expressed herein do not necessarily state or reflect those of the United States government or Lawrence Livermore National Security, LLC, and shall not be used for advertising or product endorsement purposes.

Comparing Plasma Conditions in Short-Pulse-Heated Foils via Fine-Structure X-ray Emission[a)]

B. F. Kraus,[1,2,b)] A. Chien,[1,2] Lan Gao,[2] K. W. Hill,[2] M. Bitter,[2] P. C. Efthimion,[2] Hui Chen,[3] M. B. Schneider,[3] A. Moreau,[4] R. Hollinger,[4] Shoujun Wang,[4] Huanyu Song,[4] and J. J. Rocca[4,5]

[1)] *Department of Astrophysical Sciences, Princeton University, Princeton, New Jersey, USA*

[2)] *Princeton Plasma Physics Laboratory, Princeton University, Princeton, New Jersey, USA*

[3)] *Lawrence Livermore National Laboratory, Livermore, California, USA*

[4)] *Electrical and Computer Engineering Department, Colorado State University, Fort Collins, Colorado, USA*

[5)] *Physics Department, Colorado State University, Fort Collins, Colorado, USA*

(Dated: 16 December 2020)

Fine-structure x-ray spectra have been measured from foils with embedded tracer layers at two laser facilities. A suite of layered foils with thin Ti tracers under varied tamper layers were studied at both the Titan and the ALEPH 400 nm laser facilities, where Ti Heα emission was recorded by a high-resolution Bragg crystal spectrometer. Several indicators of plasma parameters are examined in the spectra, including temperature- and density-dependent line ratios and line broadening from Stark and opacity effects. Inferences of plasma conditions are consistent with differing levels of temporal contrast at each laser facility.

I. INTRODUCTION

X-ray emission spectroscopy is a key diagnostic for understanding laser-produced plasmas, especially near solid density where lower energy photons cannot escape the plasma. Even with coarse spectral resolution, x-ray line intensity ratios that depend on ion charge state have been used to derive electron temperature profiles, informing theories of electron transport[1] and shock heating[2]. However, many physical effects can be responsible for line ratios and lineshapes, including Stark microfields[3], dielectronic recombination[4], plasma collisions[5], and radiation transport[6]. Leveraging these known correlations to diagnose plasma parameters has been difficult in the high-energy-density (HED) regime due to plasma gradients and insufficient spectral resolution, both of which blur the requisite fine-structure line emission.

Recently, high-resolution Bragg crystal spectrometers have been deployed to study laser-produced plasmas[7]. With spectral resolving power $E/dE \sim 10^4$, crystal spectrometers can distinguish x-ray lines from fine-structure transitions and their detailed lineshapes. When coupled with target platforms that spatially limit relevant emission to thin tracer layers, minimizing the impact of plasma gradients, this new diagnostic capability enables laboratory tests of HED plasma physics, collisional-radiative equilibria, and atomic physics models.

This work compares high-resolution crystal spectrometer data captured at two two laser facilities, thereby showcasing several techniques that relate fine-structure x-ray spectra to plasma parameters. The techniques show that specific line ratios, sensitive to either electron temperature or collisionality, can corroborate inferences from independently analyzed lineshapes, sensitive to either Stark or opacity broadening. The four spectral indicators compose a consistent narrative regarding the plasma conditions created by the two lasers: at the Titan laser, a high-intensity prepulse expands the plasma, lowering its density and heating deeper layers; whereas at the ALEPH laser, extreme temporal contrast minimizes plasma pre-expansion, maintaning near-solid density and restricting electron heating to a thinner surface region. This interpretation builds confidence that many aspects of fine-structure x-ray spectra can be reliable diagnostics of hot, near-solid-density plasmas.

II. EXPERIMENTAL DETAILS

A. Crystal spectrometer design

Optimized x-ray spectrometers that capture fine-structure emission from HED plasmas must satisfy two requirements: they must diffract photons energetic enough to escape solid-density plasmas (generally, > 1 keV) with high spectral resolution, and they must overcome the strong particle and photon noise ubiquitous in HED experiments. The first requirement is best achieved with perfect crystals such as quartz, Ge, or Si, which have relatively small atomic spacing (for high-energy photons) and narrow rocking curves (for high spectral resolution); quartz is particularly useful because it can be cut to accommodate a wide variety of atomic spacings without forbidden reflections[8]. The second requirement is achieved by bending crystals into focusing

---

[a)] Contributed paper published as part of the Proceedings of the Virtual 23rd Topical Conference on High-Temperature Plasma Diagnostics hosted by Los Alamos National Laboratory.

[b)] Electronic mail: bkraus@pppl.gov

geometries, where spherically bent crystals are especially versatile for minimizing source-size broadening, maintaining high throughput, and fitting into constraining vacuum chamber geometries.

For these reasons, a spherically bent quartz $(21\bar{3}1)$ crystal of dimension 30×50 mm^2 was chosen to diffract x rays of interest near 4.73 keV at a Bragg angle $\theta_B \sim 58.2°$. The radius of curvature 49 cm is tight enough to fit the focusing spectrometer geometry inside meter-scale vacuum chambers, without being so tight that crystal properties are severely affected. The integrated crystal rocking curve is estimated by XOP[9] to be 26.6 μrad, setting an upper limit on spectral resolution of $E/dE \sim 6 \times 10^4$; in practice, the resolution is determined by the detector pixel size and source size broadening.

B. Tracer layer targets

The spectroscopic tracer material was chosen to be Ti for several reasons: it is highly ionized at achievable temperatures $T_e \sim 1$ keV, its $n = 2 \rightarrow 1$ Heα resonance line at 4.75 keV can escape dense plasmas, it has many non-overlapping satellite transitions to Heα, and it is easy to embed in targets via sputtering. Thin Ti layers were deposited on Al foils of thickness 20–25 μm, and subsequently covered by a second tamper layer of Al. Both tracer and tamper layers had variable thicknesses, with Ti tracers of 125, 250, 500, or 1000 nm and Al tampers between 0 and 4 μm. The thickness of the Ti tracer layer sets the volume of plasma visible by the spectrometer, so it therefore balances signal (enhanced for thick layers) against plasma homogeneity (gradients are minimized for thin layers). The tracer thickness also governs the importance of radiation transport, since photons must traverse more absorbing material before they emerge. On the other side, varying the tamper layer changes the relative depth of the Ti layer with respect to the foil surface where the laser interaction occurs. Therefore, a scan over tamper layer thickness maps the characteristics of emitted x-ray spectra versus tracer layer depth.

C. Deployment at laser facilities

Both of the laser facilities examined in this work have short pulse durations < 1 ps and relativistic intensities $> 10^{18}$ W/cm^2, but their characteristics create starkly different plasma conditions. The Titan laser at the Jupiter Laser Facility delivers > 100 J of 1053 nm, 1ω light to a laser focus with $\varnothing \sim 20$ μm in 700 fs, and a strong prepulse deposits $\gtrsim 1$ mJ over several ns before the main pulse. By contrast, the ALEPH 400 nm beamline[10] sends 8–10 J of 2ω light to a diffraction-limited spot with $\varnothing \sim 1$ μm in 45 fs. Due to frequency doubling, laser has extremely high temporal contrast (10^{-12} at 25 ps). The difference in prepulse intensity strongly impacts the condition of the target when the main pulse arrives.

Spectrometer deployment strategy was influenced by the target chamber geometry and noise considerations. At Titan, a large vacuum chamber with 1 m radius necessitated placing the entire spectrometer inside the chamber, so an adjustable-angle crystal mount was constructed for easy alignment[7]. Because the detector was in the same chamber as the laser-target interaction, particle and photon noise were significant; spectrometers viewing near target normal required all-direction shielding, including contributions from thick plastic, Pb bricks, and Ta sheets. Image plate detectors, with 100 μm pixels that capped the resolution near $E/dE \sim 10^4$ and a readout system that required venting each shot cycle, were the only feasible detector option. At the ALEPH facility, a smaller chamber with 70 cm radius accommodated an external crystal box; a vacuum-tight crystal holder was machined with the precise Bragg angle and tilt necessary to focus Ti x rays onto a 25×25 mm^2 CCD with (13.5 μm)^2 pixels, installed outside the chamber and requiring only a thin Al foil filter to eliminate visible photon noise. Because the CCD remained fixed in space over the duration of the experiment (unlike image plates, which can shift by mm with each replacement), the spectral dispersion was consistent for all target configurations, and each experiment could be repeated to build photon statistics.

In both cases, the spherical crystal was set up in a focusing geometry, with the crystal center between 85 and 110 cm from the interaction and the detector between 38 and 42 cm from the crystal. (A similar layout is pictured in Ref. 7.) This geometry is advantageous because the detector is near the Rowland circle for the central diffracted wavelength, minimizing source size broadening; however, the small x-ray emitting volumes already make this degradation to spectral resolution negligible, especially in a defocusing geometry.

III. X-RAY INDICATORS OF PLASMA PARAMETERS

X-ray spectra were obtained from a variety of target configurations at each laser facility. Data here from Titan comes from a single shot, whereas ALEPH data represents the average of 10 identical shots. For each focused x ray image, a one-dimensional intensity spectrum is constructed by integrating along the sagittal (spatial) dimension. The spectral dispersion that converts detector position to energy is first approximated by an analytical function describing this focusing geometry, with inputs such as θ_B and source-to-crystal distance, and is then tuned by matching several clear satellite transition lines with their known energies.

A. Whole-spectrum Stark broadening

Two spectra from comparable targets at each facility are shown in Fig. 1. Using Gabriel's notation to label each transition[11], the spectra encompass the 1s2p ^{1}P$_1 \rightarrow$

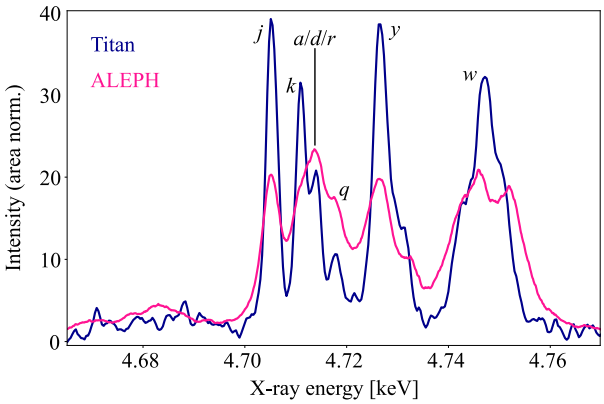

FIG. 1. Measurements of the full Ti Heα spectrum, captured at Titan (blue) and ALEPH (pink), from targets with 0.5 µm Ti tracer layer and 1.25 µm Al tamper.

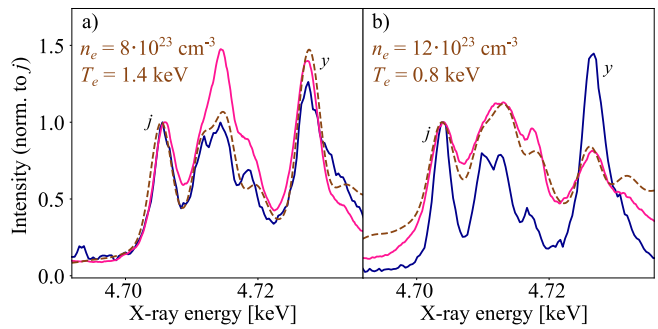

FIG. 2. Experimental satellite spectra (blue solid: Titan; pink solid: ALEPH) compared to SCRAM calculations (brown dashed) at the noted n_e and T_e. a) Spectra from targets with 0.6 µm Al tamper. b) Spectra from targets with ≥ 2.5 µm Al tamper.

$1s^2\ ^1S_0$ resonance transition (w) and its He-, Li-, and Be-like satellites at lower energies. Many discrepancies between the spectra are immediately evident regarding both line widths and line ratios.

Though many physical mechanisms affect only particular lines and not others, it is apparent that *all* line widths are broader in data from ALEPH. This enhanced width is observed in both optically thick (w) and optically thin satellite lines (such as j and k), indicating that it is not solely caused by opacity broadening. A more feasible cause that would affect all line widths is Stark broadening by plasma particle microfields, where increased plasma density leads to more broadening[3]. Many features of the ALEPH spectrum, such as the blurring of shoulder q compared to a or the half-width-half-maximum of the isolated j line, could be compared to synthetic lineshapes from Stark microfield simulations to quantify the higher plasma density; even without such models, the spectra imply that the hot plasma density at ALEPH is substantially higher than at Titan.

B. Temperature from satellite ratios

Of the satellite lines on the red side of the Ti Heα resonance, several are chiefly excited via dielectronic recombination (DR), a process which relies on resonant electron capture and therefore depends on electron temperature T_e. The j satellite line, one of the strongest (and here, most isolated) transitions caused mostly by DR, has been used to diagnose temperatures in tokamak plasmas[4] and can be interpreted similarly here. In principle, j can arise from electron collisions with pre-excited Li-like levels $1s^22p$, but this effect is only predicted to be important for j at densities far above solid[5]. We nonetheless balance DR with all other excitation mechanisms by employing a collisional-radiative model.

The spectra shown in Fig. 2 capture conditions from shallow tracer layers (a) and deeper tracer layers (b). In each case, a collisional-radiative calculation from SCRAM[12] is overlaid. Both comparisons show a similar intensity ratio of the He-like y line to the DR j line between the ALEPH data and SCRAM calculation. The data indicates that the line ratio y/j decreases dramatically with tracer layer depth at ALEPH; at Titan, however, y/j remains high even under microns of material. With increasing temperature, the importance of DR decreases, so that the ratio y/j increases with T_e. From this perspective, both lasers create hot material ($T_e > 1$ keV) near the foil surface, but T_e at ALEPH decreases almost $2\times$ under 2.5 µm of tamp. The temperature gradient at Titan is much smaller.

We note that these line ratios had much higher shot-to-shot variation at Titan than they did at ALEPH.

C. Density from $a + d$ intensity

The nature of satellite excitation depends on the atomic physics of each transition and which plasma effects are relevant in a given regime. For example, at low plasma densities, all x-ray transitions decay much faster than electron-ion collision times, so there is no mechanism other than DR to excite autoionizing $1s2p^2$ levels. As densities and therefore collision frequencies increase, low-energy collisions become plentiful enough to equilibrate the ground configuration $1s^22s$ with the excited $1s^22p$ configuration. In this case, all states $1s^22\ell$ are in local thermodynamic equilibrium, opening a new route via high-energy collisions to the doubly excited $1s2p^2$ configuration. In the Heα spectrum, the satellites first affected by this collisionality effect are a, b, c and d[5].

In the Ti Heα spectrum, a and d are exactly overlapping in energy, but since their intensity is determined by the same mechanism, we loosely treat them here as a single line. (Note that r shares the same energy, but its intensity scales with and is smaller than q and it is therefore inconsequential here.) It is clear in Fig. 3 that the $a + d$ line is systematically higher in all spectra from

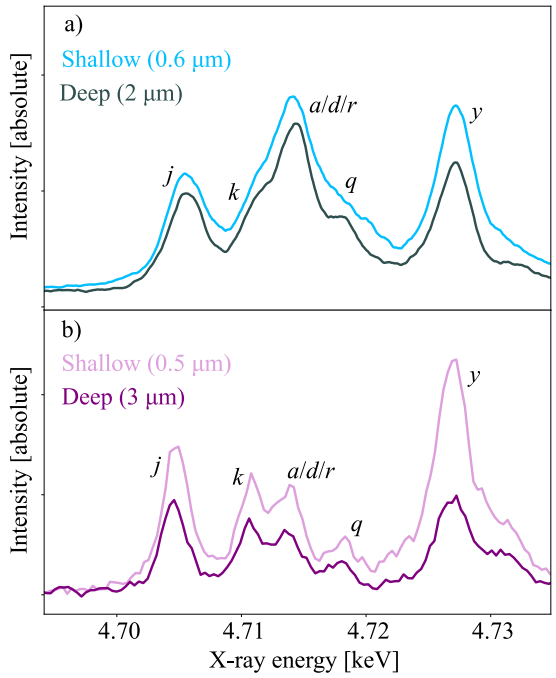

FIG. 3. Experimental satellite spectra from (a) ALEPH and (b) Titan. Al tamp thickness is shown for each spectrum, with lighter (darker) lines for shallower (deeper) tracer layers.

ALEPH (a) than from Titan (b). The spectra in the figure are representative; other than a few measurements from shallow tracer layers at Titan with probable Doppler shift contamination, the satellites $a + d$ are always more intense than j at ALEPH and less intense than j at Titan. This discrepancy for this particular satellite is noticeably absent for other Li-like satellites, signaling that collisionality and therefore plasma density is substantially higher at ALEPH than at Titan.

D. Opacity of the w resonance line

Dense plasmas have enhanced capacity to absorb resonant photons through photoexcitation, with the strongest lines most susceptible. In the data here, the w resonance line has by far the highest opacity κ. Fig. 4 shows highly resolved lineshapes of the w line alone for various targets at ALEPH (a,b) and Titan (c). Fig. 4(a) shows a scan over tamper layer thickness, with w decreasing in relative intensity with tracer layer depth. Given a similar charge state distribution (as expected, since He-like ions exist for wide T_e ranges), κ is proportional to ion density n_i, and the decreasing w intensity corresponds to an increasing n_i with tracer layer depth.

The optical depth $\tau = \kappa L$ is defined as the number of photon mean free paths required to traverse a material of thickness L. The emergent w lineshape should thus appear more opaque and decrease in intensity as the tracer layer thickness L increases. This scan is performed at ALEPH (Fig. 4(b)) and Titan (4(c)), both of which show clear and monotonic trends as expected. However, the character of the lineshapes is evidently different for ALEPH versus Titan. Firstly, the line widths are noticeably broader at ALEPH; secondly, the ALEPH lineshapes show a self-reversed dip at the line center (emphasized with the arrow in Fig. 4(b)). Both qualities are predicted opacity effects: absorption is strongest at the resonant line energy and decreases rapidly in the wings, so that photons further from line center are more likely to escape. The self-reversed feature is a hallmark of opaque plasmas with $\tau \gg 1$[6,13]. These features of the w lineshapes from ALEPH indicate that κ is significantly higher than at Titan, implying that n_i is higher at ALEPH than at Titan.

IV. DISCUSSION

Several findings have been independently corroborated by different aspects of the Ti Heα spectrum at Titan and ALEPH. Firstly, the plasma density at ALEPH is significantly higher than at Titan, and secondly, T_e is high for near-surface layers at both facilities but drops more quickly at ALEPH. These two differences between the facilities are consistent with the drastically higher temporal contrast at the ALEPH laser. With less than 10^{-11} J on target within 25 ps of the main pulse, the ALEPH 400 nm beam ensures that the foil target is largely intact when the bulk of the laser energy arrives. As such, the target is heated and highly ionized well before plasma ablation expands tracer layers, so that the time-integrated x-ray signals presented here emit from a near-solid-density plasma. In comparison, the Titan laser has much more laser energy (> 1 mJ) impact the target before the main pulse, with much of this energy arriving nanoseconds early. These prepulse photons drive plasma ablation for a long enough period to considerably expand the ultimate short-pulse target compared to the initially solid foil. Highly charged ions heated by the main pulse will therefore exist in a much lower density, pre-ablated plasma than they would with higher temporal contrast.

The lower density at Titan, as corroborated by narrower line widths, a less intense $a + d$ satellite, and a less opaque w resonance, is a direct consequence of the high-intensity prepulse and subsequent pre-expansion. The behavior of the y/j line ratio, indicating high (but less repeatable) T_e in deeper layers at Titan than at ALEPH, is also consistent with plasma pre-expansion, since the critical density plane where most laser energy is deposited moves inward from its initial position on the foil surface. Therefore, the tracer layers may experience more heating due to being closer to the location of laser-plasma interaction. Furthermore, prepulse characteristics tend to vary shot-to-shot because of strong but often unknown dependence on many laser parameters. Therefore, the lack of repeatability in inferred T_e at the Titan laser is reasonable to associate with prepulse variation.

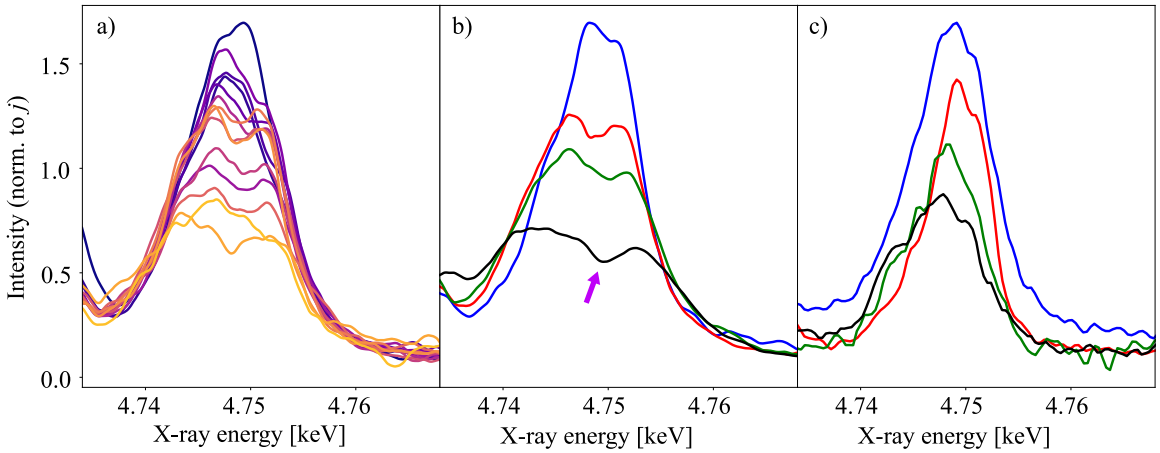

FIG. 4. The w resonance lineshape with intensity normalized to optically thin j (not shown). (a) A scan at ALEPH with 0.25 µm Ti tracer layers and Al thickness increasing from purple to yellow. (b) A scan at ALEPH with constant 1 µm Al tamper and varied tracer layer thickness: 125 nm (blue), 250 nm (red) 500 nm (green), 1 µm (black). (c) A similar scan over tracer layers at Titan with 2 µm Al tamper and tracer layers 250 nm (blue), 500 nm (red), 1 µm (green), and 6 µm (black).

All measurements presented here are integrated over space and time. The thin tracer layers build spatial resolution into a suite of measurements over different targets, but motion of the emitting thin layers during ablation occurs over µm or less, making imaging challenging. On the other hand, obtaining time-resolved similar measurements would be straightforward by coupling the focusing spectrometer with a streak camera, some of which can resolve evolving emission spectra with sub-ps resolution.

Quantifying plasma parameters from fine-structure spectra often requires sophisticated models, from plasma microfield lineshape calculators to collisional-radiative predictions of line intensities. Such modeling is continually progressing[14,15] and there is often significant scatter in estimates of spectral quantities by different methods. Highly resolved measurements from near-solid-density plasmas may direct the development of these models in a challenging regime, and may eventually provide benchmarks when corroborated by secondary diagnostics.

This work has reviewed several indicators of plasma conditions present in high-resolution x-ray spectra from HED plasmas. These measurements have been performed at two short-pulse laser facilities and are consistent with expected plasma conditions, illustrating the capacity of high-resolution x-ray spectra to diagnose a variety of hot plasmas near solid density.

ACKNOWLEDGEMENTS

This work was performed under the auspices of the U.S. Department of Energy by Princeton Plasma Physics Laboratory under contract DE-AC02-09CH11466 and by Lawrence Livermore National Laboratory under contract DE- AC52-07NA27344. One experimental campaign was supported by DOE Office of Science, Fusion Energy Sciences under Contract No. DE-SC-0019076: the LaserNetUS initiative at the Advanced Beam Laboratory.

[1] C. Brown, D. Hoarty, S. James, D. Swatton, S. Hughes, J. Morton, T. Guymer, M. Hill, D. Chapman, J. Andrew, *et al.*, Phys. Rev. Lett. **106**, 185003 (2011).
[2] K. Akli, S. Hansen, A. Kemp, R. Freeman, F. Beg, D. Clark, S. Chen, D. Hey, S. Hatchett, K. Highbarger, *et al.*, Phys. Rev. Lett. **100**, 165002 (2008).
[3] E. Stambulchik and Y. Maron, High Energy Density Phys. **6**, 9 (2010).
[4] M. Bitter, K. Hill, M. Zarnstorff, S. Von Goeler, R. Hulse, L. Johnson, N. Sauthoff, S. Sesnic, K. Young, M. Tavernier, *et al.*, Physical Review A **32**, 3011 (1985).
[5] V. Jacobs and M. Blaha, Phys. Rev. A **21**, 525 (1980).
[6] R. D. Cowan and G. H. Dieke, Rev. Mod. Phys. **20**, 418 (1948).
[7] H. Chen, M. Bitter, K. Hill, S. Kerr, E. Magee, S. Nagel, J. Park, M. Schneider, G. Stone, G. Williams, *et al.*, Rev. Sci. Instrum. **85**, 11E606 (2014).
[8] X.-R. Huang, T. Gog, J. Kim, E. Kasman, A. H. Said, D. M. Casa, M. Wieczorek, M. G. Hönnicke, and L. Assoufid, J. Appl. Crystallography **51**, 140 (2018).
[9] M. S. del Río and R. J. Dejus, in *Adv. Comp. Meth. X-Ray Optics II*, Vol. 8141 (International Society for Optics and Photonics, 2011) p. 814115.
[10] Y. Wang, S. Wang, A. Rockwood, B. M. Luther, R. Hollinger, A. Curtis, C. Calvi, C. S. Menoni, and J. J. Rocca, Optics Lett. **42**, 3828 (2017).
[11] A. Gabriel, Mon. Not. Royal Astr. Soc. **160**, 99 (1972).
[12] S. Hansen, J. Bauche, C. Bauche-Arnoult, and M. Gu, High Energy Density Phys. **3**, 109 (2007).
[13] F. Irons, J. Phys. B: Atomic and Molecular Phys. **8**, 3044 (1975).
[14] S. Alexiou, E. Stambulchik, T. Gomez, and M. Koubiti, Atoms **6**, 13 (2018).
[15] S. B. Hansen, H.-K. Chung, C. J. Fontes, Y. Ralchenko, H. Scott, and E. Stambulchik, High Energy Density Phys. **35**, 100693 (2020).